Jim Lambers
ENERGY 281
Spring Quarter 2007-08
Lecture 8 Notes

These notes are based on Rosalind Archer's PE281 lecture notes, with some revisions by Jim Lambers.

1 Constant Pressure Inner Boundary Condition

The previous two solutions have considered constant rate boundary conditions at the well. It is also possible to consider constant pressure boundary conditions. It becomes more convenient to define the dimensionless pressure, p_D, in terms of both the initial reservoir pressure, p_i, and the well pressure, p_w:

$$p_D = \frac{p_i - p}{p_i - p_w} \tag{1}$$

The dimensionless form of the pressure equation is as before:

$$\frac{1}{r_D}\frac{\partial}{\partial r_D}\left(r_D\frac{\partial p_D}{\partial r_D}\right) = \frac{\partial p_D}{\partial t_D} \tag{2}$$

For an infinite acting reservoir, the boundary and initial conditions in dimensionless form are

$$p_D(1, t_D) = 1, \tag{3}$$

$$\lim_{r_D\to\infty} p_D(r_D, t_D) = 0, \tag{4}$$

$$p_D(r_D, 0) = 0. \tag{5}$$

As before, the general solution to this problem is

$$\hat{p}_D(r_D, s) = c_1(s)I_0(r_D\sqrt{s}) + c_2(s)K_0(r_D\sqrt{s}) \tag{6}$$

Again, c_1 is set to zero to ensure the pressure remains finite as $r_D \to \infty$. The inner boundary condition is used to solve for c_2. We have

$$\hat{p}_D(1, s) = c_2(s)K_0(\sqrt{s}) = \frac{1}{s} \tag{7}$$

which yields

$$c_2(s) = \frac{1}{sK_0(\sqrt{s})}. \tag{8}$$

and

$$\hat{p}_D(r_D, s) = \frac{K_0(r_D\sqrt{s})}{sK_0(\sqrt{s})}. \tag{9}$$

The inverse transform to solve this problem was provided by Van Everdingen and Hurst, "The Application of the Laplace Transformation to Flow Problems in Reservoirs", Petroleum Transactions AIME, 305-324, 1949 (see equation VI-26):

$$p_D(r_D, t_D) = \frac{2}{\pi}\int_0^\infty \frac{(1 - e^{-u^2 t_D})[J_0(u)Y_0(ur_D) - Y_0(u)J_0(ur_D)]}{u^2[J_0^2(u) + Y_0^2(u)]}\, du. \tag{10}$$

Recall that J_0 is a Bessel function of the first kind, and Y_0 is a Bessel function of the second kind.

1.1 Early Time Behavior of the Flow Rates

Just as the early time behavior of the pressure could be considered in the constant flow rate case, the behavior of the flow rate can be examined for the constant pressure case. Applying the Laplace transform to both sides of

$$q_D = -r_D \frac{\partial p_D}{\partial r_D} \tag{11}$$

yields

$$\hat{q}_D = -r_D \frac{\partial \hat{p}_D}{\partial r_D} = -r_D \frac{\partial}{\partial r_D}\left(\frac{K_0(r_D\sqrt{s})}{sK_0(\sqrt{s})}\right) \tag{12}$$

Using the previously established expression for the derivative of K_0 gives

$$\hat{q}_D(r_D, s) = \frac{r_D}{\sqrt{s}}\frac{K_1(r_D\sqrt{s})}{K_0(\sqrt{s})}. \tag{13}$$

The *cumulative recovery* is defined by

$$Q_D(r_D, t_d) = \int_0^{t_d} q_D(r_D, t_D)\, dt_D. \tag{14}$$

The Laplace transform of Q_D can be found readily by recalling Theorem 7:

$$\hat{Q}_D(r_D, s) = \frac{1}{s}\hat{q}_D(r_D, s) = \frac{r_D}{s^{\frac{3}{2}}}\frac{K_1(r_D\sqrt{s})}{K_0(\sqrt{s})}. \tag{15}$$

To consider the early time behavior of the flow rates, consider the limit of q_D as $s \to \infty$. The early time behavior of the Bessel functions have already been established:

$$K_1(r_D\sqrt{s}) \approx \sqrt{\frac{\pi}{2\sqrt{s}r_D}}e^{-r_D\sqrt{s}}, \tag{16}$$

$$K_0(\sqrt{s}) \approx \sqrt{\frac{\pi}{2\sqrt{s}}} e^{-\sqrt{s}}. \tag{17}$$

It follows that

$$\hat{q}_D(r_D, s) = \frac{r_D}{\sqrt{s}} \sqrt{\frac{\pi}{2\sqrt{s} r_D}} e^{-r_D\sqrt{s}} \sqrt{\frac{2\sqrt{s}}{\pi}} e^{\sqrt{s}} = \frac{\sqrt{r_D}}{\sqrt{s}} e^{-\sqrt{s}(r_D-1)} \tag{18}$$

q_D can now be found by using the Maple function `invlaplace`:

$$q_D(r_D, t_D) = \frac{\sqrt{r_D}}{\sqrt{\pi t_D}} e^{-\frac{(r_D-1)^2}{4t_D}}. \tag{19}$$

Q_D (at early time) can also be found by using `invlaplace`:

$$Q_D(r_D, t_D) = \sqrt{r_D} \left\{ 2\sqrt{\frac{t_D}{\pi}} e^{-\frac{(r_D-1)^2}{4t_D}} - (r_D - 1)\text{erfc}\left(\frac{r_D - 1}{2\sqrt{t_D}}\right) \right\}. \tag{20}$$

Note the similarity between this and

$$p_D(r_D, t_D) \approx \frac{1}{\sqrt{r_D}} \left\{ 2\sqrt{\frac{t_D}{\pi}} e^{-\frac{(r_D-1)^2}{4t_D}} - (r_D - 1)\text{erfc}\left(\frac{r_D - 1}{2\sqrt{t_D}}\right) \right\}, \tag{21}$$

the early time behavior of the pressure for constant rate, finite radius well.

2 Bounded Reservoir Example

The previous examples have considered flow in infinite acting reservoirs. Linear boundaries in reservoirs with either constant pressure or constant flow rate wells can be created using superposition as discussed in Lecture 1. Consider a case with a constant flow rate and the well and a constant pressure at the outer boundary (at radius r_e). The boundary and initial conditions in dimensionless form are:

$$r_D \left.\frac{\partial p_D}{\partial r_D}\right|_{r_D=1} = -1, \tag{22}$$

$$p_D(r_{De}, t_D) = 0, \quad r_{De} = \frac{r_e}{r_w}, \tag{23}$$

$$p_D(r_D, 0) = 0, \quad \forall r_D. \tag{24}$$

As before, the general solution to this problem is

$$\hat{p}_D(r_D, s) = c_1(s) I_0(r_D\sqrt{s}) + c_2(s) K_0(r_D\sqrt{s}). \tag{25}$$

However, in this example, the reservoir is bounded, so $c_1(s)$ can not be set to zero by arguing that $\hat{p}_D$ must remain bounded as r_D tends to infinity.

Instead, the outer boundary condition requires:

$$c_1(s)I_0(r_{De}\sqrt{s}) + c_2(s)K_0(r_{De}\sqrt{s}) = 0. \tag{26}$$

The inner boundary conditions requires

$$\frac{\partial}{\partial r_D}[c_1(s)I_0(r_D\sqrt{s}) + c_2(s)K_0(r_D\sqrt{s})]\Big|_{r_D=1} = -\frac{1}{s}. \tag{27}$$

The derivatives of the Bessel functions can be found from

$$\frac{d}{dx}[x^{-n}K_n(x)] = -x^{-n}K_{n+1}(x), \tag{28}$$

$$\frac{d}{dx}[x^{-n}I_n(x)] = x^{-n}I_{n+1}(x). \tag{29}$$

Using these derivatives, (27) becomes

$$c_1(s)\sqrt{s}I_1(\sqrt{s}) - c_2(s)\sqrt{s}K_1(\sqrt{s}) = -\frac{1}{s} \tag{30}$$

$$\implies \quad c_1(s)I_1(\sqrt{s}) - c_2(s)K_1(\sqrt{s}) = -\frac{1}{s^{\frac{3}{2}}}. \tag{31}$$

Equations (31) and (26) can be solved for c_1 and c_2 to give

$$c_1(s) = -\frac{1}{s^{\frac{3}{2}}}\frac{K_0(r_{De}\sqrt{s})}{K_0(r_{De}\sqrt{s})I_1(\sqrt{s}) + K_1(\sqrt{s})I_0(r_{De}\sqrt{s})}, \tag{32}$$

$$c_2(s) = \frac{1}{s^{\frac{3}{2}}}\frac{I_0(r_{De}\sqrt{s})}{K_0(r_{De}\sqrt{s})I_1(\sqrt{s}) + K_1(\sqrt{s})I_0(r_{De}\sqrt{s})}. \tag{33}$$

It follows that

$$\hat{p}_D(r_D, s) = \frac{1}{s^{\frac{3}{2}}}\frac{I_0(r_{De}\sqrt{s})K_0(r_D\sqrt{s}) - K_0(r_{De}\sqrt{s})I_0(r_D\sqrt{s})}{K_0(r_{De}\sqrt{s})I_1(\sqrt{s}) + K_1(\sqrt{s})I_0(r_{De}\sqrt{s})}. \tag{34}$$

The late time (steady state) behavior of p_D can be determined by taking the limit of $\hat{p}_D$ as s tends to zero. We use the approximation

$$I_v(x) \approx \frac{1}{\Gamma(v)+1)}\left(\frac{x}{2}\right)^v \tag{35}$$

to obtain

$$\hat{p}_D(r_D, s) \approx \frac{1}{s^{\frac{3}{2}}}\frac{-\ln r_D + \ln r_{De}}{\frac{1}{2}(-\ln(r_{De}\sqrt{s})/2 - \gamma)\sqrt{s} + 1/\sqrt{s}} \to \frac{1}{s}\ln\frac{r_{De}}{r_D} \tag{36}$$

which yields

$$p_D(r, t_D) \to \ln\frac{r_{De}}{r_D}. \tag{37}$$

3 Incorporating Dual Porosity

In dual porosity reservoirs, flow occurs in both the matrix and in the fractures. Their are two important parameters in dual porosity reservoirs:

$$\omega = \frac{\phi_f c_{tf}}{\phi_f c_{tf} + \phi_m c_{tm}}, \quad 0 < \omega < 1, \tag{38}$$

$$\lambda = \alpha \frac{k_m}{k_f} r_w^2, \quad 10^{-10} < \lambda < 10^{-3}, \tag{39}$$

where α depends on the fracture configuration e.g. sugar cube model.

The governing equation in Laplace space for a dual porosity reservoir is

$$\frac{1}{r_D} \frac{\partial}{\partial r_D} \left(r_D \frac{\partial \hat{p}_D}{\partial t_D} \right) - s f(s) \hat{p} = 0, \tag{40}$$

where

$$f(s) = \frac{s\omega(1-\omega) + \lambda}{s(1-\omega) + \lambda}. \tag{41}$$

For the case of an infinite acting reservoir with a finite radius, the solution for $\hat{p}_D$ is

$$\hat{p}_D = \frac{K_0(r_D \sqrt{sf(s)})}{s\sqrt{sf(s)} K_1(\sqrt{sf(s)})}. \tag{42}$$

For more details see "Well Test Analysis", Rajagopal Raghavan, Englewood Cliffs, 1993.

4 Bourgeois and Horne

Marcel Bourgeois completed an MS degree in the Department of Petroleum Engineering in 1992 ("Well Test Interpretation Using Laplace Space Type Curves"). This was a key contribution to the use of Laplace transforms in well testing. The solutions to many well testing problems (beyond the examples presented here) are known in Laplace space. As part of his study, Bourgeois defined a quantity known as the Laplace pressure, $s\hat{p}$. When plotted against $1/s$, this has similar behavior as the real pressure.

Bourgeois showed that instead of performing parameter estimation using nonlinear regression in real space, the matching could be achieved efficiently and effectively in Laplace space. The efficiency lies in the removal of the need for a numerical inverse transform to evaluate the performance of set of paramter estimates. In Bourgeois' examples, fewer iterations were needed when matching in Laplace space than in real space.

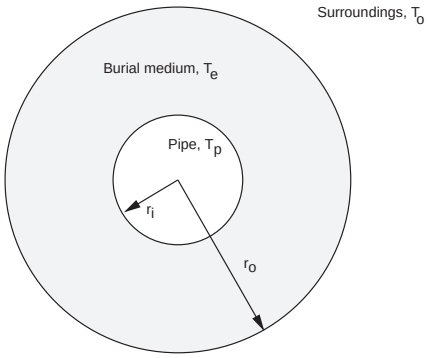

Figure 1: Configuration of pipe and surrounds

5 Heat Transfer

Laplace transforms are also useful in other petroleum engineering engineering problems. Consider heat transfer from a buried pipeline which connects an offshore platform to onshore production facilities. Heat transfer is a particular concern, because the fluids can form solid hydrates if the temperature falls below a critical level.

The pipe is buried below the sea floor. This makes the computational domain semi-infinite. However, in the part of the study that used Laplace transforms, an "effective cylinder" configuration was used as shown in Figure 1.

Two energy balance equations are required in this problem. The first governs the temperature distribution in the pipe surrounds:

$$k_e \nabla^2 T_e = \rho_e c_e \frac{\partial T_e}{\partial t}. \tag{43}$$

The second energy balance governs the fluid in the pipe which is flowing at velocity U:

$$\rho_p c_p \frac{\partial T_p}{\partial t} + \rho_p c_p U \frac{\partial T_p}{\partial x} = -\frac{2}{r_i} q, \tag{44}$$

where q is the flux of heat through the pipe wall:

$$q = -k_e \left. \frac{\partial T_e}{\partial r} \right|_{r=r_i}. \tag{45}$$

The solution procedure involves solving for the Laplace transform of T_e in

terms of T_p. This expression is then substituted into the equation governing the Laplace transform of T_p. Finally, $\hat{T}_p$ is solved for.

An example of this solution given below for the case of the pipeline heating up at start-up:

$$\hat{T}_p(x,s) = \frac{T_i - T_o}{s} \exp\left[-\left(\frac{s}{U} + \frac{2k_e\sqrt{s\kappa}\gamma}{r_i\rho_p c_p U\theta}\right)x\right] + \frac{T_o}{s} \tag{46}$$

where

$$\theta = K_0(\sqrt{s\kappa}r_i)I_0(\sqrt{s\kappa}r_o) - K_o(\sqrt{s\kappa}r_o)I_0(\sqrt{s\kappa}r_i), \tag{47}$$

$$\kappa = \frac{\rho_e c_e}{k_e}, \tag{48}$$

$$\gamma = K_0(\sqrt{s\kappa}r_0)I_1(\sqrt{s\kappa}r_i) + K_1(\sqrt{s\kappa}r_i)I_0(\sqrt{s\kappa}r_o). \tag{49}$$

The transient pipeline temperature distribution could be found by numerically inverting the expression for $\hat{T}_p$. The results from this approach were much closer to field test results than results from a large finite difference simulation. Since the numerical inverse can be computed very quickly, many more cases could be considered to assess the sensitivities to various parameters in the model.

6 Numerical Inversion of Laplace Transforms

The inverse Laplace transform can also be written as an integral:

$$f(t) = \mathcal{L}^{-1}\{F(s)\} = \frac{1}{2\pi i}\int_{\gamma-i\infty}^{\gamma+\infty} e^{st}F(s)\,ds, \tag{50}$$

where γ is chosen in such away that any singularities in $F(s)$ are avoided. The contour the integral is performed over is known as the Bromwich contour. When an inverse transform is required that can't be found from tables, this integral is usually evaluated numerically.

The most commonly used algorithm for numerical inversion of Laplace transforms is the Stehfest algorithm (Communications of the Association for Computing Machinery, algorithm 368). To invert $\hat{f}(s)$, the following summation is performed:

$$f(t) = \frac{\ln 2}{t}\sum_{i=1}^{N} V_i \hat{f}\left(\frac{\ln 2}{t}i\right) \tag{51}$$

where

$$V_i = (-1)^{\frac{N}{2}+i} \sum_{k=\lfloor \frac{i+1}{2} \rfloor}^{min(i,N/2)} \frac{k^{\frac{N}{2}}(2k)!}{(N/2-k)!k!(k-1)!(i-k)!(2k-i)!}. \qquad (52)$$

Theoretically, the accuracy of $f(t)$ increases as N increases. However, in practice, the V_i grow quickly in magnitude with N and round-off errors are amplified. Usually, $N = 8$ is used in numerical inversions. This means that for every value of $f(t)$, 8 values of $\hat{f}(s)$ are required.

The Stehfest algorithm works well for smooth functions, but has difficulties for oscillatory functions and functions with discontinuities. Oscillatory functions can be inverted if their wavelength is large with respect to half the width of the peaks. Stehfest tested his algorithm on 50 functions and reported errors of only 0.1%.

There are other algorithms available for the numerical inversion of Laplace transforms. The Talbot algorithm (J. Inst. Math. Appl., Jan. 1979, pg 97-120) is one of the most accurate and widely applicable. Other algorithms seek to reuse previously evaluated $\hat{f}(s)$ values in the evaluation of subsequent $f(t)$ values.